University of Pittsburgh

ORTHOPAEDIC ROBOTICS LABORATORY

2016 summer undergraduate abstract booklet

PITT | SWANSON ENGINEERING
BIOENGINEERING

FOREWORD

The Orthopaedic Robotics Laboratory is the University of Pittsburgh's collaborative effort between the Department of Bioengineering and Department of Orthopaedic Surgery. The mission of the ORL is the prevention of degenerative joint disease by improving diagnostic, repair, and rehabilitation procedures for musculoskeletal injuries using state-of-the-art robotic technology. The ORL would like to commend the work of the undergraduate students during the summer of 2016. Students made significant impacts in the study of hand, shoulder, and knee joint diseases. The work of our students, with the help of our mentors, contributes greatly to the world of orthopaedic research.

Our team

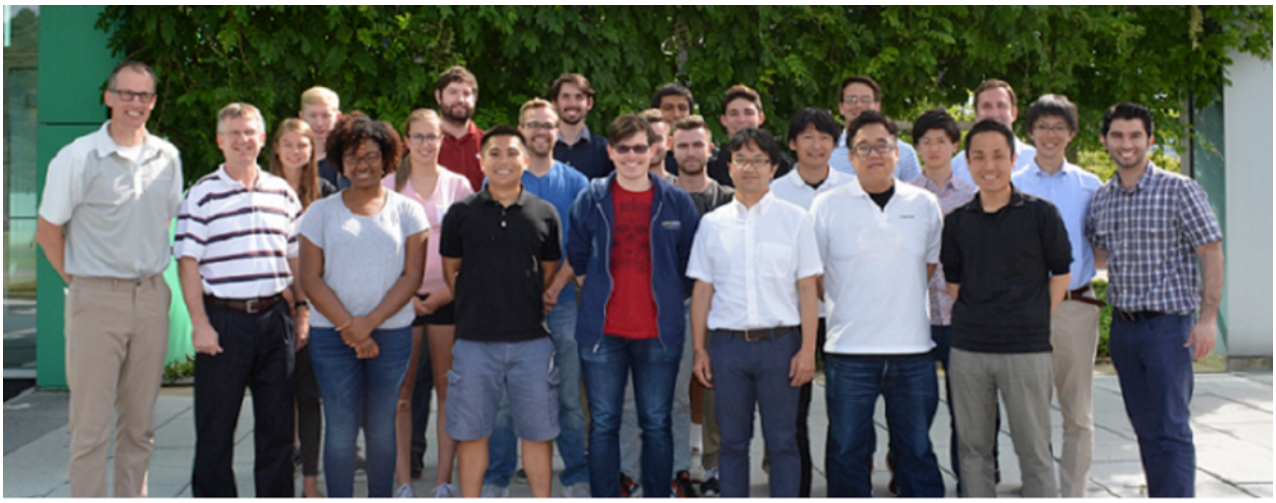

Chris Como
Class of 2017
Bioengineering
University of Michigan

Ryan Black
Class of 2018
Bioengineering
University of Pittsburgh

Emily Anthony
Class of 2017
Mechanical Engineering
University of Pittsburgh

Patrick Haggerty
Class of 2017
Bioengineering
University of Pittsburgh

Jackie Schauble
Class of 2018
Bioengineering
University of Pittsburgh

Samik Patel
Class of 2018
Bioengineering
University of Pittsburgh

Table of contents

Predicting Mechanical Properties with Quantitative Ultrasound Measures

Black, RT[1]; Ferrer, GA[1]; Yoshida, M[2]; Musahl, V[2,1]; Debski, RE[1,2]
1. Department of Bioengineering, University of Pittsburgh, Pittsburgh, PA, United States
2. Department of Orthopaedic Surgery, University of Pittsburgh, Pittsburgh, PA, United States

Introduction: Ultrasound is a common imaging modality used to evaluate musculoskeletal tissues non-invasively and dynamically [1]. Tissue geometry can be assessed objectively, but determining tissue quality is largely subjective. As a result, clinical ultrasonography examinations have low repeatability between examiners [1]. Previous studies have proposed the use of quantitative ultrasound measures (QUS) to objectively evaluate tissue quality using ultrasound imaging [1,4,5]. In addition, studies have shown that better tendon quality is correlated with QUS measures including higher values of echogenicity and variance and lower values of skewness and kurtosis [4]. However, the relationship between these QUS measures and mechanical properties of musculoskeletal tissues, which are representative of tissue quality, are poorly understood. Therefore, the objective of this study is to relate mechanical properties of human tendon with QUS measures to be able to quantify tendon quality. It was hypothesized that high values of echogenicity and variance and low values of skewness and kurtosis are related to greater mechanical properties representing better tissue quality.

Methods: Five fresh frozen cadaveric long head of biceps tendon (LHBT) were harvested from intact shoulder specimens (59.8 ± 9.6 years old). The LHBT was then dissected into a "dog-bone" shape approximately half the width of the tendon to ensure failure in the midsubstance [2,3]. Two rubber band markers were superglued to the tendon at the ends of the "dog-bone" region to provide a point of reference to ensure repeatability between ultrasound images (Fig. 1). Using a laser scanner (Next Engine, Desktop 3D Scanner, Santa Monica, CA, USA), the cross-sectional area of the "dog-bone" region of the tendon was measured [2]. The LHBT was then secured to the materials testing machine (Instron Model 5965, Norwood, MA, USA) for uniaxial tensile testing using soft tissue clamps. A layer of skin was wrapped around the tendon to allow for ultrasound imaging during mechanical testing. For mechanical testing, a 1N preload was applied to the LHBT, followed by preconditioning from 1-10N for 20 cycles at 10 mm/min. After preconditioning, the LHBT was loaded from 1-30N for 50 cycles at 10 mm/min. The max load of a loading set was then increased by 20N until tendon failure occurred (ie. 1-30N, 1-50N, etc.). Following each loading set, three ultrasound images (GE, LOGIQ S8, Fairfield, CT, USA) were taken at the max load of each loading set by a single experienced ultrasound examiner using a rig designed to ensure repeatable placement of the ultrasound probe. For each ultrasound image, a region of interest (ROI) was selected as a box centered between the rubber band markers (Fig. 1). QUS measures (Skewness, Kurtosis, Variance, Echogenicity) were calculated from a grayscale distribution produced from the ROI [1,4,5]. QUS measures from each of the three ultrasound images taken for a loading set were adjusted to account for baseline QUS measures of surrounding, unloaded fat tissue. Mechanical

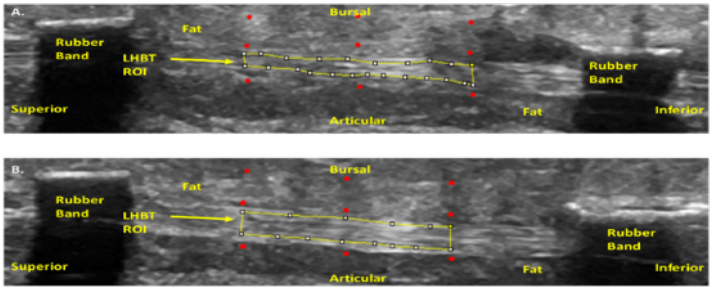

Figure 1: Typical Ultrasound images of LHBT obtained. The ROI for the LHBT is defined by the yellow box in the images. A) Ultrasound image at 15 MPa located within the toe region of the stress strain curve. B) US image at 28 MPa located within the linear region of the stress strain curve.

properties including toe region tangent modulus and linear region tangent modulus were determined using the last cycle of the stress strain curve for each loading set, while creep was determined using the last and initial cycles of the stress strain curve for each loading set. A backwards multiple linear regression was performed to test the influence of QUS measures on mechanical properties of the tendon. Significance was set at $p < 0.05$.

Results: A significant multiple linear regression model was found for each mechanical property determined in this study involving the interaction of at least two QUS measures as predictors (Table 1). Both creep and linear region tangent modulus were predicted by the interaction between kurtosis and variance, while toe region tangent modulus was predicted by the interaction between skewness, kurtosis, and variance. The sign of the beta coefficient indicates the type of relationship between the variables (ie. positive is direct relationship, negative is inverse relationship). For example, creep was found to be inversely proportional to kurtosis and variance (Creep = (-6.21)(Kurtosis) + (-0.05)(Variance) + 26.98), thus decreasing kurtosis and variance were related to increasing creep. There were no other significant multiple linear regression models between the mechanical properties (Creep, Toe Region Tangent Modulus, Linear Region Tangent Modulus) and the QUS measures (Skewness, Kurtosis, Variance, Echogenicity).

Discussion: Previous studies have shown that different measures of tissue quality individually correlate with single QUS measures [4].The results of this study show that the interaction of multiple QUS measures can predict mechanical properties, representative of tissue quality. Both creep and linear region tangent modulus were shown to be inversely related to kurtosis and variance, while toe region tangent modulus was shown to be directly related to skewness and inversely related to kurtosis and variance. These results do not support our initial hypothesis, however the interaction between multiple QUS measures as predictors of mechanical properties influences the relationships observed between the QUS measures and mechanical properties. In the future, other musculoskeletal tissues, including rotator cuff tendons, will be assessed using QUS measures to determine tissue quality. These QUS measures will provide clinicians with a repeatable tool to predict mechanical properties of musculoskeletal tissue using ultrasonography, providing insight on tissue quality and microstructure.

Significance: Clinicians will be able to use QUS measures to better assess mechanical properties of musculoskeletal tissue, representative of tissue quality, with ultrasonography, a common, inexpensive, and dynamic imaging modality, to improve treatments.

References: [1] Collinger J et al. Academic Radiology. 2009; 16:1424-1432. [2] McGough R et al. Knee Surg, Sports Traumotol, Arthroscopy. 1996; 3:226-229 [3] Kolz C et al. Clinical Biomechanics. 2015; 30:940-945. [4] Collinger J et al. Am. J. Phys. Med. Rehabil. 2010; 89:390-400. [5] Collinger J et al. PM R. 2010; 2:920-925.

Creep (%)			
Predictors	**Beta Coefficients**	**Intercept**	**R^2**
Kurtosis	-6.21	26.98	0.595
Variance	-0.05		

Toe Region Tangent Modulus			
Predictors	**Beta Coefficients**	**Intercept**	**R^2**
Skewness	458.68	529.42	0.540
Kurtosis	-235.74		
Variance	-0.55		

Linear Region Tangent Modulus			
Predictors	**Beta Coefficients**	**Intercept**	**R^2**
Kurtosis	-105.38	852.95	0.309
Variance	-0.53		

Table 1: Summary of multiple linear regression analysis performed between QUS measures and mechanical properties.

Influence of Bone Mineral Density & Insertion Torque on ACL Soft Tissue Graft Fixation with Interference Screws

Chris J. Como[1], Elmar Herbst[1], Thomas Pfeiffer[1], Jan-Hendrik Naendrup[1], Volker Musahl[1], Richard E. Debski[1]

[1]Orthopaedic Robotics Laboratory, University of Pittsburgh, Pittsburgh, PA

Disclosures: Chris J. Como (N), Elmar Herbst (N), Thomas Pfeiffer (N), Jan Hendrik Naendrup (N), Volker Musahl (N), Richard E. Debski (N)

Introduction: Due to the increased athletic participation of middle-aged and elderly people, more sports related injuries have occurred for these age groups. When performing surgery on these patients, surgeons must consider a possibly decreased bone mineral density (BMD) [1]. Following anterior cruciate ligament (ACL) reconstruction procedures, the graft fixation strength needs to withstand forces during physical therapy as well as strenuous activities once the patient returns to sports because the graft is not yet fully incorporated [2]. Particularly when using interference screws, the graft fixation strength depends on bone mineral density of the subjects and insertion torque of the interference screw [3, 4]. However, the influence of different screw sizes has not been examined. Therefore, the purpose of this study was to investigate the influence of bone mineral density and insertion torque on load-to-failure and stiffness of two interference screws for ACL soft tissue graft fixation. Based on prior studies that investigated the screw geometry [5], it was hypothesized that oversizing the interference screw by one millimeter relative to the bone tunnel diameter will result in a higher load-to-failure and stiffness compared to an interference screw matching the bone tunnel diameter.

Methods: Fourteen fresh-frozen cadaveric knees (mean age 52.6 +/- 12.1 yrs) were randomly assigned to one of the following screw conditions: 1) sized interference screw matching the bone tunnel and graft diameter, 2) one millimeter oversized interference screw compared to the bone tunnel and graft diameter. All interference screws had a length of twenty-five millimeters. To determine the BMD of each specimen, DXA scans (GE Healthcare Lunar iDXA Madison, WI) of the lateral femoral condyle were performed. A bone socket within the native ACL footprint was drilled according to the size of the graft to a depth of twenty-five millimeters, and the quadrupled autologous hamstring tendon grafts were inserted. A torque screwdriver (0.2 N-m – 4.5 N-m) recorded the insertion torque. The bone was potted in epoxy putty and mounted to a materials testing machine (Instron® 5965 Dual Column Testing System). The tibial end of the graft was clamped at a distance of three centimeters from the femoral tunnel aperture to simulate the intra-articular graft length. The longitudinal axis of the bone tunnel was then aligned to the applied force.

Specimens were preloaded with 10 N, followed by 20 cycles of preconditioning between 10 and 50 N. Cyclic creep was performed between 10 and 250 N to replicate forces in the ACL graft during walking [6]. Load-to-failure testing at 20 mm/min was then performed. Load-to-failure and stiffness were recorded. A correlation analysis for each group was performed with the Pearson correlation coefficient to evaluate the correlation of both insertion torque and bone mineral density with the maximum load-to-failure. A student's t-test was used to compare the

results between the two groups. The significance level was set at $p < 0.05$.

Results: A significant correlation between bone mineral density and load-to-failure ($R = 0.770$, $p = 0.043$) was found for the sized screw condition, such that higher bone mineral density corresponded to higher load-to-failure. A strong, but not significant correlation was found for the oversized screw ($R = 0.682$, $p = 0.204$) (Figure 1). A strong correlation between insertion torque and load-to-failure for both the sized screw condition ($R = 0.811$, $p = 0.027$) and the oversized screw condition ($R = 0.522$, $p = 0.229$) was found. Strong, but not significant correlations were found between insertion torque and stiffness for both sized ($R = 0.654$, $p = 0.111$) and oversized screws ($R = 0.519$, $p = 0.233$). Between the two groups, only insertion torque was found to be significantly different ($p = 0.012$), whereas BMD ($p = 0.679$), load-to-failure ($p = 0.286$), and stiffness ($p = 0.397$) did not differ significantly between the sized and oversized screw conditions (Table 1).

Discussion: The most important finding of this study is that both bone mineral density and insertion torque strongly correlate with load-to-failure and stiffness of ACL soft tissue graft fixation. We also found that load-to-failure depends less on BMD for the oversized screw condition, likely due to the overstuffing of the graft and screw in the bone tunnel. Even though load-to-failure and stiffness were found to be higher in the oversized screw condition, no significant difference was found, partially disproving our hypothesis. It has previously been shown that insertion torque correlates positively with load-to-failure and stiffness. However, until now surgeons could not quantify the insertion torque and relied on their subjective feeling during insertion of interference screws. Using a torque screwdriver to determine insertion torque may help to provide an objective method for surgeons to determine proper fixation and to interpret the graft fixation intraoperatively and modify this for another fixation method. To fully understand the influence of BMD on ACL soft tissue graft fixation, additional fixation devices (i.e., extra-cortical suspensory fixation techniques) need to be investigated.

Significance: The results of this study will provide surgeons with useful information to help determine the optimal fixation technique for an ACL reconstruction based on bone mineral density and insertion torque. Oversized interference screws produce a higher load-to-failure and stiffness than sized screws, which may prove to be useful in treating patients with particularly low bone mineral densities.

References:

[1] Cvijetić, Selma, Mirko Koršić. *Osteoporosis International* 2004; [2] Mündermann A, et al. *J Orthop Res* 2015; [3] Gallo RA, et al. *Knee* 2015; [4] Brand JC, et al. Am J Sports Med 2000; [5] Weiler A, et al. *Am J Sports Med* 2000; [6] Shelburne KB, et al. *J Biomech* 2004

Table 1: Bone mineral density (BMD), insertion torque, load-to-failure, and stiffness for sized and oversized screws (mean ± SD; *p < 0.05)

Specimen	BMD (g/cm²)	Torque (N-m)	Load-to-Failure (N)	Stiffness (N/mm)
Sized	1.178 ± 0.324	1.4 ± 0.4*	410.6 ± 151.0	111.6 ± 40.2
Oversized	1.234 ± 0.097	2.3 ± 0.7*	506.2 ± 168.8	133.0 ± 50.4

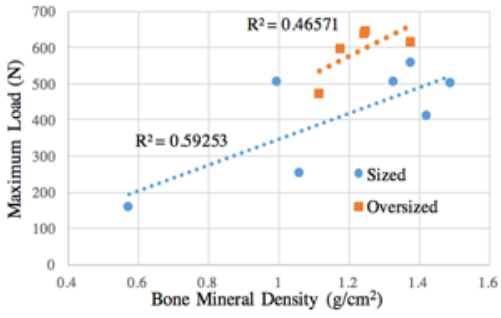

Figure 1: Correlation of BMD to maximum load for screw conditions

Impact of Screw Length on Fixed Proximal Scaphoid Fracture Biomechanics: In Vitro Study with Cyclic Loading and Load to Failure

Samik Patel, Juan Giugale MD, Nathan Tiedeken MD, Richard E. Debski PhD, Robert Kauffman MD, John Fowler MD

Orthopaedic Robotics Laboratory, Department of Bioengineering, University of Pittsburgh, PA, USA

Introduction: Internal fixation used as treatment for scaphoid fractures has increased with advances in surgical techniques [1]. Proximal pole scaphoid fractures present a clinical challenge due to their lower success rate when cast immobilization and internal fixation are utilized [2]. Screws maximizing length have been shown to impact wrist motion for fixed scaphoid waist fractures [3]. Additionally, screws with greater diameters and varying geometry have been shown to impact stiffness and ultimate load at the fracture site for fixed scaphoid waist fractures. Currently, the effect of screw length on the structural properties of fixed proximal scaphoid fractures is not well understood even though fixation of proximal scaphoid fractures has a high nonunion rate. Therefore, the objective of this study is to determine the bending stiffness and ultimate load for the loading of fixed proximal scaphoid fractures for screws of various lengths.

Methods: Fifteen, fresh frozen cadaveric scaphoids (57.6±10.3 years of age) underwent an oblique osteotomy with a .52mm blade saw to simulate a 7mm proximal oblique fracture with respect to the long axis. Each scaphoid was randomly assigned for fixation to one of 3 possible screw lengths (n=5) of a 2.5mm diameter central threadless screw (Stryker, Kalamazoo, MI, USA): 10mm, 18mm, and 24mm length. The distal pole of the scaphoids was potted in epoxy putty (Bondo, St. Paul, MN, USA) with the scaphoid long axis perpendicular to the horizontal plane. The scaphoid was then oriented at 45° to simulate clinical dorsal to volar bending load (Figure 1).

Each specimen was cyclically loaded for 1000 cycles with an 800Nmm bending moment, where the applied load (40.0N-66.7N) depended on the moment arm between the potting and a plunger driven by a materials testing machine (Instron, Eden Prairie, MN). Stiffness was calculated at the 1000^{th} cycle and cyclic failure was defined as either plunger extension greater than 2.5mm or a proximal pole crack in the construct [4]. Each specimen was loaded to failure after cyclic loading. Failure was indicated by loss of fracture reduction or a proximal crack in the construct as a result of loading (Figure 2); this was defined by as a distinct decrease in the load-displacement curve.

One-way analysis of variance (ANOVA) tests were performed to evaluate differences in stiffness and load to failure. Significance was set at $p<0.05$.

Results: No significant difference in long axis lengths between the randomized groups of scaphoids was found. Additionally, no significant difference in stiffness at the 1000^{th} cycle between different screw lengths was found (Figure 3). All specimens with 18mm and 24mm screw fixations were able to withstand cyclic loading, however 1 specimen fixed with a 10mm screw failed during cyclic loading. As a result, a proximal fracture fixed with a 10mm screw was able to withstand 845 ± 346 cycles. Load to failure was significantly ($p<.05$) impacted by screw length utilized for fixation. A significant difference ($p<.05$) in load to failure between a 10mm screw and 24mm screw was found, however no significant difference ($p=.606$) occurred in load to failure between an 18mm and 24mm screw (Figure 3).

Discussion: This study examined the effect of screw length on bending stiffness during cyclic loading and load to failure. The results of this study show that a screw that maximizes the length (24mm) within a specimen withstands significantly greater load to failure than a screw that is centered (10mm) with respect to the fracture site. The 10mm screw gains less purchase in the bone on either side of the fracture compared to the 24mm screw. However, there is no statistically significant difference in load to failure between an 18mm screw, that does not maximize its length within the specimen, and a 24mm screw; this could be occurring because the 18mm screw is more centered with respect to the screw compared to the 24mm screw. Our data contradicts a previous study that contends that maximizing the screw length significantly optimizes wrist biomechanics and fracture healing [3].

Significance: The results of this study will provide surgeons with useful information that will help them in determining an optimal screw length for the fixation of

proximal scaphoid fractures using central threadless screws. Fixation utilizing an 18mm screw compared to a 24mm screw minimizes the risk for injury to the distal radius articulation during surgery.

References:

[1] Rhemrev SJ et al. Int J Emer Med. 2011; 4:4.

[2] Trumble M et al. J Amer Soc Surg H. 2001; 155-171.

[3] Dodds SD et al J Hand Surg Am. 2006; 405-413 [4] McCallister WV et al. J Bone Joint Surg Am. 2003;72-77

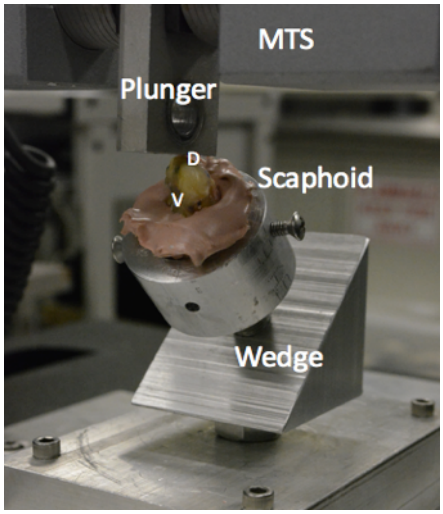

Figure 1: Experimental setup with the distal scaphoid potted in the epoxy putty. Bending load was applied with a plunger attached to a materials testing machine. The scaphoid was oriented at a 45° angle.

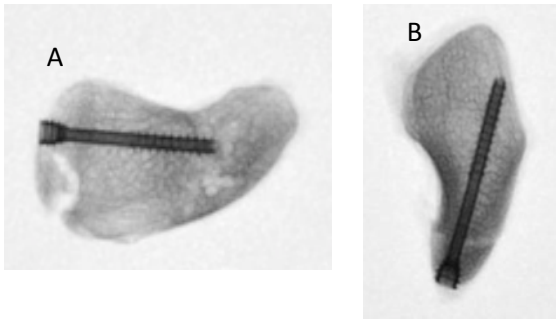

Figure 2A: Displays failure by proximal crack.

Figure 2B: Displays failure by loss of fracture reduction.

Screw Length	Stiffness (N/mm)	Load to Failure (N)
10mm (n=5)	209.2±40.2	180.5±83.2 *
18mm (n=5)	220.9±55.6	319.0±95.4
24mm (n=5)	236.7±37.4	437.2±68.5 *

Figure 3: Stiffness at the 1000th cycle during cyclic loading of an 800 Nmm bending moment and load to failure withstood based on screw length utilized for fixation. (mean ± SD, *p<.05)

Quantification of Cellularity and Lipoid Degeneration to Assess Localized Degeneration in Rotator Cuff Tendons

Schauble, JA[1,2]; Miller, RM[1,2]; Musahl, V[1,2]; Debski, RE[1,2]

1. Orthopaedic Robotics Laboratory, Pittsburgh, PA,

Introduction: Degenerative rotator cuff tears are a common problem, affecting greater than 30% of the general population [1]. Rotator cuff tears most commonly occur in the supraspinatus tendon near the insertion site [2]. There is a high failure rate of rotator cuff tear repairs, and this failure typically occurs at the tendon-suture interface [3]. By determining localized differences in rotator cuff tendon degeneration, surgical techniques can be improved. Past studies have evaluated localized tendon degeneration, but these studies only focused on one location in the tendon, such as the medial edge of a chronic tear [2]. Therefore, the objective of this study is to evaluate localized tendon degeneration in multiple locations by quantifying cellularity and lipoid degeneration, two characteristics of tendon degeneration. It was hypothesized that there would be more lipoid degeneration in the supraspinatus than the infraspinatus, and that there would be more cellularity in tendons with chronic tears than in intact tendons.

Methods: Eight fresh-frozen cadaveric shoulders were used in this study. Four shoulders were intact (55 ± 12 years) and four had small tears in the supraspinatus tendon (70 ± 9 years). Tissue biopsy samples were taken from the anterior and posterior sides of the insertion, mid-substance, and myotendinous junction regions on the supraspinatus tendon. Samples were also taken from the infraspinatus, in the same regions as the supraspinatus. For specimens with a chronic tear, samples were also taken from the medial edge. The samples were fixed in a 10% buffered formalin solution for at least three days. Then samples were sectioned at a thickness of 5 µm and cut longitudinally, stained with hematoxylin and eosin (H&E) to visualize tendon morphology, and imaged using a light microscope with a 20x objective lens across the full tendon thickness. All images were evaluated based on cellularity and lipoid degeneration. To quantify cellularity, the number of nuclei in each sample was counted using ImageJ software. For lipoid degeneration analysis, ImageJ software was utilized to determine the percent area of lipoid degeneration per sample. A two-way ANOVA and a post-hoc test was conducted to compare degeneration based on location and whether the specimen had a tear, with a significance of $p < 0.05$. Degeneration comparing the supraspinatus vs. infraspinatus and intact vs. chronic tear were performed using a paired t-test.

Results: While tendons showed varying degrees of degeneration, there was no statistical significance between the supraspinatus and infraspinatus based on lipoid degeneration. It was also found that there was no statistical significance between intact and chronic tears based on cellularity, thus disproving both hypotheses. However, there was a significant interaction effect between location and the presence of a tear for cellularity ($p=0.016$). The tendon mid-substance showed significantly more cellularity in specimens with chronic tears when compared to intact tendons, ($p=0.024$) [Fig 1B, Fig 2]. Tendons with chronic tears showed significantly more lipoid degeneration in the myotendinous junction when compared to intact tendons ($p=0.006$) [Fig 1C, Fig 3].

Discussion: The results of this study showed that tissue degeneration is spread throughout the tendon, and is not localized to one specific location. As lipoid degeneration was very high for tendons with chronic tears in the myotendinous junction, and cellularity was high for chronic tears at the mid-substance, it can be concluded that degeneration and the presence of a tear are linked factors. Increased cellularity can be a result of inflammation, and lipoid degeneration could be due to muscle atrophy, both associated with tendon injury. Both

of these degeneration parameters can serve as a potential reason for the high suture pull out rates in rotator cuff repairs. This study is significant because high amounts of degeneration can result in reduced material properties, which can lead to a chronic tear and further tendon degeneration. This is clinically significant because surgeons should avoid areas of poor tissue quality when performing a rotator cuff repair. Although the results did not support the hypotheses, the results showed that increases in localized tendon degeneration are not limited to the medial edge of the tear. Future directions for this study include evaluating nuclei shape to determine differences in localized degeneration.

Significance: Through understanding the linkage between chronic rotator cuff tears and localized tendon degeneration, surgical techniques can be improved so that regions of high degeneration are not used in a rotator cuff repair.

References:

[1] Yamamoto J Shoulder Elbow Surg. 2010 Jan;19(1):116-20.

[2] Sano H et al. J Shoulder Elbow Surg. 1999;8(6):574-9.

[3] Ponce et al. Am J Sports Med. 2013;41(10):2256-61.

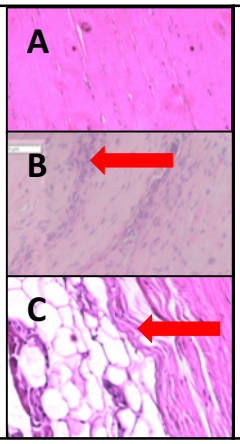

Fig. 1: Histological images of rotator cuff tendons. A) Intact infraspinatus tendon mid-substance with healthy cells and no lipoid degeneration B) Chronic tear supraspinatus tendon exhibiting hypercellularity. C) Chronic tear infraspinatus myotendinous junction showing

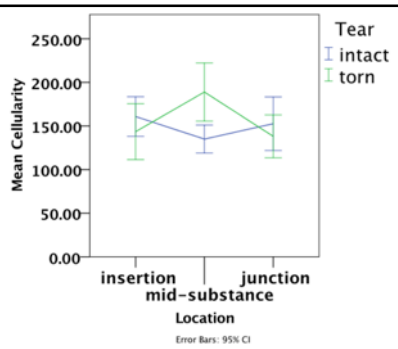

Fig. 2: Mean cellularity for each sample location for intact and torn tendons.

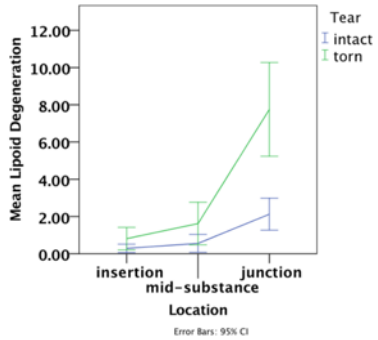

Fig. 3: Mean lipoid degeneration for each sample location for intact and torn tendons.

Utilizing a 3D Motion-Tracking System for the Biomechanical Analysis of Distal Tibiofibular Kinematics

Patrick J. Haggerty[1], Thomas R. Pfeiffer[1], Conor I. Murphy[1], Joseph P. Russell[1], Richard E. Debski[1], Macalus V. Hogan[1]

[1]Orthopaedic Robotics Laboratory, Department of Orthopaedic Surgery, Department of Bioengineering, University of Pittsburgh

INTRODUCTION

Injuries to the ankle syndesmosis are fairly common, accounting for approximately 5-10% of all ankle sprains and 23% of all ankle fractures [1]. The most common mechanisms for syndesmotic injuries are external rotation and/or hyper-dorsiflexion of the ankle, both of which may disrupt the syndesmotic ligaments and compromise the integrity of the distal tibiofibular complex. Surgical fixation of the fibula to the tibia attempts to stabilize the fibula as well as allow the distal ligaments to repair properly. However, current fixation methods are relatively ineffective, resulting in extended recovery times and patient reports of ankle pain and discomfort [2]. Thus, there is a need to examine syndesmotic injuries in order to improve surgical fixation methods of the distal fibula. Previous studies of syndesmosis injuries and fixation methods have used specimens in which the lower-leg is sectioned, thereby disrupting the proximal tibiofibular syndesmosis. In addition, these studies used manually applied loads and static trials, which are not ideal for testing. The MJT Model FRS2010 robotic testing system at the Orthopaedic Robotics Laboratory is designed for 6-DOF biomechanical joint testing, and is capable of precise motion and dynamic loading. Even so, the robotic testing system is only able to track tibiotalar motion, so to quantify tibiofibular motion an external tracking system is necessary. One effective technique of analyzing syndesmotic injury is by observing 6-DOF fibular motion with respect to the tibia in various intact, injury, and fixation models for cadaveric specimens. This motion can be determined by defining coordinate systems for the tibia and fibula and finding the relationships between those coordinate systems. This requires usage of an external tracking system which can define and track the tibia and fibula as rigid bodies in a three dimensional space. The objective of this project was to develop and validate an experimental setup through which distal tibiofibular antero-posterior (AP) translation, medio-lateral (ML) translation, and transverse rotation (TV) could be quantified via a 3D motion-tracking system.

SUCCESS CRITERIA The system is able to return translation values at an accuracy better than1 mm and rotation values at an accuracy better than 2^{o}.

FINAL DESIGN

The final experimental setup consists of a combination between the MJT Model FRS2010 robotic testing system and the OptiTrack 3D motion-tracking system. The robotic testing system is used to assure rigidity by fixing the lower leg in place and to precisely externally rotate and invert the foot by applying dynamic forces and moments. The final OptiTrack system is comprised of 6 infrared-based cameras situated in a hemispherical fashion around the specimen, an OptiTrack calibration wand, ground plane, two dissimilar reflective marker triads, and digitizer. All OptiTrack accessories (wand, plane, markers, digitizer) are fitted with reflective markers which allows them to be recognized by the camera system.

PROTOCOL

Robotic Testing System: Two sets of marker triads are rigidly mounted to the lower-leg: one on the tibia, one on the fibula. The lower-leg is then rigidly fixed perpendicular to the lower plate of the robotic testing system (MJT Model FRS2010, Chino, Japan) and the ankle is rigidly fixed to a plate connected to the robotic manipulator via a universal force/moment sensor (UFS, ATI Delta IP60 (SI-660-60) Apex, NC). Once the specimen is properly fastened to the robot, a Microscribe (Microscribe MX, Solution Technologies Inc., Oella, MD) is used to test rigidity of the construct.

OptiTrack Motion-Tracking System: After mounting and initial rigidity testing of the specimen, six OptiTrack cameras (Flex 13, NaturalPoint Inc., Corvallis, Oregon) are situated around the specimen at various heights and depths. Ambient light in the testing space is minimized. Motive (Motive:Tracker, NaturalPoint Inc, Corvallis, Oregon), the accompanying motion-tracking software package of OptiTrack, is booted, and a project is initiated. A calibration wand (CWM-250, NaturalPoint Inc., Corvallis, Oregon) is waved around the specimen and throughout the desired capture volume to calibrate the camera system and render a 3D capture volume in Motive. A ground plane (CS-200 Calibration Square, NaturalPoint Inc., Corvallis, Oregon) is placed on the lower plate of the robotic testing system to define a global coordinate

system for reference. The dissimilar marker triads fastened to the tibia and fibula are then identified within Motive's 3D capture volume and are defined as distinct rigid bodies with distinct coordinate systems (Figure 1). For each rigid body, Motive automatically tracks translations and rotations and formulates exportable transformation matrices. After rigid body definition, an OptiTrack digitizer with reflective markers is calibrated by fixing its corresponding calibration block (Figure 2) to the lower plate of the robot, placing the digitizer tip in one of the calibration holes (marked A, B, C, and D) and moving the digitizer in a hemisphere around the block while keeping the tip fixed. Once calibration is complete the digitizer is used to define four anatomical positions: the lateral malleolus, tibiotalar joint center, tibial tuberosity, and Gerdys tubercle. From the last three positions, a tibial anatomical coordinate system is generated. A fibular coordinate system is easily defined from the tibial coordinate system by shifting the origin of the tibial coordinate system (the tibiotalar joint center) to the tip of the lateral malleolus. The digitizer is still in its beta stages of testing and is not yet integrated into OptiTrack systems, so custom MATLAB (MathWorks Inc, MA) code is used to calibrate the digitizer as well as define the digitizer's local coordinate system which can be seen in Figure 2.

Data Analysis

Once calibration of the robotic and OptiTrack systems is complete, the robot is able to move the specimen through varying degrees of external rotation and inversion and the tracking system can effectively quantify the tibial and fibular marker triads' movement. Data from Motive is directly exported as an excel spreadsheet in the form of quaternion transformation matrices for the fibula and tibia. Files with data for digitizer calibration and anatomical landmarks are also exported as separate excel spreadsheets. These data sets are taken in by custom MATLAB code, and through a series of transformation matrices the translation and rotation for any given ankle state is returned.

RESULTS

Translation

Translational accuracy was evaluated by using a lower-leg sawbone model. The model was mounted by screwing the tibia into the robot's lower plate and custom ankle brace, mirroring mounting of actual cadaveric specimens. Three bolts of varying lengths were measured with dial calipers and placed sequentially between the distal tibia and fibula. After placement of each bolt, the two bones were fixed via a screw. The intact sawbone model was taken as a zero reference point. Data was collected by the OptiTrack system for intact and the addition of screws 1, 2, and 3 (Table 1). The average error in translation of the system in relation to dial caliper measurements was 0.50mm.

Rotation

As in the translational accuracy test, rotational accuracy was evaluated with a lower-leg sawbone model. The model was mounted in the robot similarly to the translation test. The fibula was detached from the tibia, and the distal head was rigidly screwed into the mechanical actuator of the robotic testing system. The proximal sawbone syndesmosis remained intact. The robotic actuator was then moved through four angles of rotation: 10^o external, 5^o external, 5^o internal, and 10^o internal. The resting state of the fibula with respect to the tibia was taken as a zero reference point for rotation. Data was collected simultaneously by the OptiTrack system and the robotic testing system for the zero reference point and all four angles of rotation (Table 1). The average error in rotation with respect to the robotic testing system's measurements was 2.6^o.

DISCUSSION

The success criteria for translation and rotation results was that the system attained accuracies smaller than 1 mm and 2^o, respectively. The average calculated translational accuracy was 0.5 mm, and all three values were bounded between 0.39 and 0.58 mm, thus the system met the established criteria for translational accuracy. However, in rotation the system returned an average error of 2.6^o, which is larger than the acceptable value (2^o) for rotation. Additionally, Table 1 shows that the errors during external rotation of the fibula (5.9 and 2.6^o) were much higher than those during internal rotation (1.2 and 0.6^o)

Sources of Error

There are several general factors which could have contributed to system holistic inaccuracies. The OptiTrack Flex 13 cameras are contrast-based, meaning their accuracy will change as the level of ambient light varies. Though efforts were made to keep ambient light to a minimum, there were still small sources of light present which may have contributed minor errors. Another factor to consider is camera orientation. OptiTrack calculates

motion of reflective markers by assimilating all of its two-dimensional camera feeds (in this case, six feeds) and extrapolating a three-dimensional space from them. Certain camera orientations are more advantageous and provide a more accurate capture volume, and even minute movements of the cameras during or between capturing marker movements can skew results. Additionally, the robotic testing system used in this study is quite large and surrounds a significant portion of the specimen, which prevents orienting the cameras to give a complete 360° view of the specimen, i.e. the ideal camera orientation for best results. There are also a few factors which may have contributed to inaccuracies in rotation specifically. One factor was that the rotational axis of the robot was slightly askew from the longitudinal fibular axis. Though the difference between the axes was small, it may have had an effect on measurements. However by examining the differences between values for the robotic and optical tracking systems, one can see that accuracy is quite low only in a state of external rotation. Both values for internal rotation fall well within the success criteria. This may be due to the physical assembly of the rotational accuracy test (Figure 3). The red circle highlights the distal tip of the fibula attached to the mechanical actuator of the robot as well as the marker triad attached slightly more proximally along the fibula's midshaft. During external rotation, it was observed that the actuator shrouded the fibular marker triad's placement from three out of the six cameras. During internal rotation, it blocked the view of one at most. This was not an issue during translational testing (Figure 4) since the robot was only used for fixation purposes. Since the number of cameras able to observe both marker triads at any given time has a direct effect on the accuracy of the system, the actuator blocking the view of half the available cameras may be the direct cause of the high errors observed in external rotation. During testing of actual specimens, the actuator is in a different orientation, so the errors observed in external rotation should not be applicable.

ACKNOWEDGMENTS

This project was supported jointly by the Department of Bioengineering and the Department of Orthopaedic Surgery at the University of Pittsburgh.

REFERENCES

[1] Van Heest, T., Injuries to the Ankle Syndesmosis, JBJS, 2014:96 603-13.

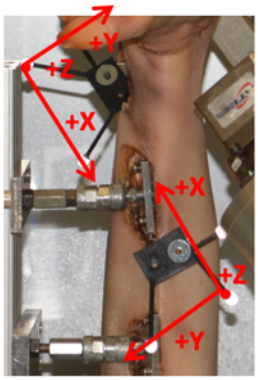

Figure 1. Reflective marker placement on tibia and fibula as well as marker coordinate systems.

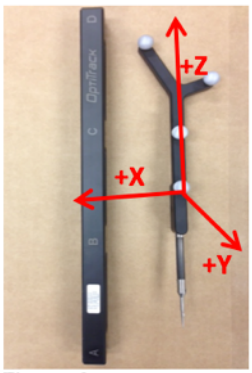

Figure 2. Digitizer and calibration block, as well as digitizer coordinate system.

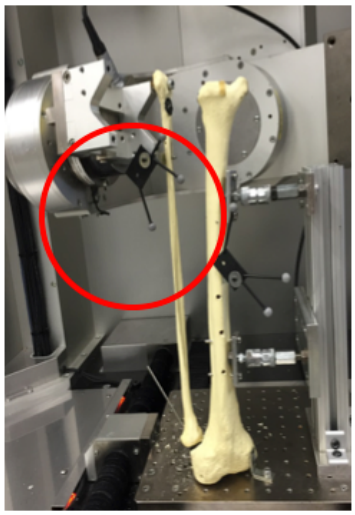

Figure 3. Experimental setup for rotational accuracy test. The actuator can be seen blocking the fibular marker triad.

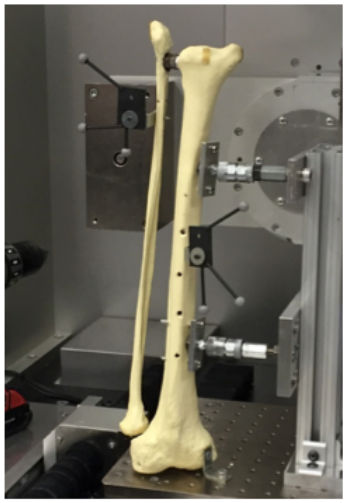

Figure 4. Experimental setup for translational accuracy test. Both triads can be seen from all camera orientations.

Translation	Dial Caliper Measurement (mm)	OptiTrack Tracking System (mm)	**Rotation**	Robotic Testing System (Degrees)	OptiTrack Tracking System (Degrees)
Reference (0 mm)	0.00	0.01	Reference (0 Degrees)	0.0	0.0
+1st nut	5.73	5.20	10 External	-10.06	-4.07
+1st and 2nd nuts	11.01	10.40	5 External	-5.06	-7.07
+ 1st, 2nd, and 3rd nuts	16.91	16.33	5 Internal	5.05	6.20
			10 Internal	10.05	10.62

Special thanks to the grad students, fellows, and residents. This booklet would not have been possible without their help and guidance along the way!